Synchronizations in small-world networks of spiking neurons: Diffusive versus sigmoid couplings

Hideo Hasegawa*
Department of Physics, Tokyo Gakugei University, Koganei, Tokyo 184-8501, Japan
(Received 22 May 2005; published 30 November 2005)

By using a semianalytical dynamical mean-field approximation previously proposed by the author [H. Hasegawa, Phys. Rev. E **70**, 066107 (2004)], we have studied the synchronization of stochastic, small-world (SW) networks of FitzHugh-Nagumo neurons with diffusive couplings. The difference and similarity between results for *diffusive* and *sigmoid* couplings have been discussed. It has been shown that with introducing the weak heterogeneity to regular networks, the synchronization may be slightly increased for diffusive couplings, while it is decreased for sigmoid couplings. This increase in the synchronization for diffusive couplings is shown to be due to their local, negative feedback contributions, but not due to the short average distance in SW networks. Synchronization of SW networks depends not only on their structure but also on the type of couplings.

DOI: 10.1103/PhysRevE.72.056139 PACS number(s): 84.35.+i, 05.45.−a, 87.10.+e, 07.05.Mh

I. INTRODUCTION

In recent years, much attention has been paid to complex networks such as small-world (SW) and scale-free (SF) networks (for a review see [1,2]). The SW network, which has been proposed by Wattz and Strogatz (WS) [3,4], is characterized by a large clustering coefficient and a small average distance. The original WS-SW network was created by introducing finite-degree heterogeneity to the regular network by random rewirings of links. Newman and Wattz (NW) [5] have proposed an alternative SW network, randomly adding shortcut links to the regular networks without rewirings. In SW networks, the degree distribution $P(k)$ for a node to have k coupled neighbors has an exponential tail for a large k. In contrast, the degree distribution in SF networks, which was first proposed by Barabási and Albert [6], is given by the power law as $P(k) \sim k^{-\gamma}$ with the index $\gamma(=2-4)$. Since Barabási and Albert [6] have proposed a growing SF network with preferential attachments of nodes, many models and mechanisms have been proposed not only for growing but also for nongrowing SF networks with geographical and nongeographical structures.

The interplay between structure and dynamics has attracted a great deal of attention to the synchronization in complex networks. The synchronization in SW networks of spiking neuron models has been studied [7–15] with the use of Hodgkin-Huxley (HH) [7,8], FitzHugh-Nagumo (FN) [9,10], Hindmarsh-Rose (HR) [11], integrate-and-fire (IF) [8,12], and phase models [13,14]. By using a more general class of models, dynamical properties including the synchrony in SW and SF networks have been also investigated [16–18]. It has been, however, controversial whether the synchronization in complex networks is better or worse than that in regular networks. Most of calculations have shown that the synchronization in SW networks is better than regular networks because of the short average distance in the former [7,11,13–16]. On the contrary, it has been shown that the average distance is not necessarily correlated with the synchronizability of the networks [10,17]. Some have claimed that the synchronization is increased or decreased depending on the adopted parameters or calculation conditions [8,9,12].

In a previous paper [10], we have developed a semianalytical theory for SW networks by generalizing the dynamical mean-field approximation (DMA) which was originally proposed for regular networks with all-to-all couplings [19,20]. The method newly developed in [10] is applicable to SW networks with a wide range of couplings covering from local to global and/or from regular to random ones. In [10], we have taken into account three kinds of spatial correlations: on-site correlation, the correlation for a coupled pair, and that for a pair without direct couplings. Our method has been applied to SW FN neural networks with sigmoid couplings [10], in which a coupling to the neuron i is given by

$$I_i^{(c)}(t) = J \sum_j c_{ij} G(x_j(t)), \tag{1}$$

where J denotes the coupling strength, $G(x)=1/\{1+\exp[-(x-\theta)/\alpha]\}$ is the sigmoid function with threshold θ and width α, and the adjacent matrix c_{ij} is $c_{ij}=c_{ji}=1$ for a coupled (i,j) pair and 0 otherwise. Calculations by the DMA and direct simulations have shown that when random links are added to regular networks, the synchronization is decreased because of the introduced heterogeneity in SW networks [10].

Besides the sigmoid coupling of Eq. (1), the diffusive coupling given by

$$I_i^{(c)}(t) = K \sum_j c_{ij} H(x_j(t) - x_i(t)) \tag{2}$$

has been widely employed for theoretical studies of neural networks, where K stands for the coupling strength and $H(x-y)$ the coupling function. Equations (1) and (2) model chemical and electrical synapses, respectively. Both chemical and electrical synapses exist in a neocortex. Chemical synapses use a chemical neurotransmitter that is packaged presynaptically into the vesicle, released in a quantized

*Electronic address: hasegawa@u-gakugei.ac.jp

amount, and binds to postsynaptic receptors. In contrast, electrical synapses are simpler in structure and function. They provide a direct pathway that allows ionic current to flow from the cytoplasm of one cell to that of another [21]. Although chemical synapses are by far the most abundant, electrical synapses also play an important role in neocortex. The purpose of the present paper is to apply the DMA to SW neural networks of FN neurons with diffusive couplings and to compare the results for diffusive couplings to those for sigmoid couplings in [10]. This is expected to provide some insight into the unsettled issue of the effect of the heterogeneity on the synchronization in SW networks mentioned above.

The paper is organized as follows. In Sec. II, we have derived differential equations (DE's), applying the DMA to SW FN networks with diffusive couplings in order to transform the original stochastic DE's to deterministic DE's. In Secs. III A and III B, we have reported numerical calculations for regular and SW networks, respectively. The final Sec. IV is devoted to conclusion and discussion.

II. SMALL-WORLD NETWORKS OF FN NEURONS

A. Adopted model and method

We have assumed that N-unit FN neurons are distributed on a ring with the average coordination number Z and the coupling randomness p. The dynamics of a single neuron i in a given SW network is described by the nonlinear DE's given by

$$\frac{dx_{1i}(t)}{dt} = F[x_{1i}(t)] - cx_{2i}(t) + I_i^{(c)}(t) + I_i^{(e)}(t) + \xi_i(t), \quad (3)$$

$$\frac{dx_{2i}(t)}{dt} = bx_{1i}(t) - dx_{2i}(t) + e \quad (i = 1 - N), \quad (4)$$

with

$$I_i^{(c)}(t) = K\sum_j c_{ij}H(x_{1j}(t) - x_{1i}(t)), \quad (5)$$

$$I_i^{(e)}(t) = A\Theta(t - t_{in})\Theta(t_{in} + t_w - t). \quad (6)$$

In Eqs. (3)–(6), $F[x(t)]=kx(t)[x(t)-a][1-x(t)]$, $k=0.5$, $a=0.1$, $b=0.015$, $d=0.003$, and $e=0$ [19,22,23]: x_{1i} and x_{2i} denote the fast (voltage) variable and slow (recovery) variable, respectively, $H(x)$ stands for the diffusive-type coupling, and c_{ij} the adjacent matrix given by $c_{ij}=c_{ji}=1$ for a coupled (i,j) pair and zero otherwise, self-coupling terms being excluded ($c_{ii}=0$). By changing the Z value, our model given by Eqs. (3)–(6) covers from local couplings ($Z \ll N$) to global couplings ($Z=N-1$). We should, however, keep in mind that the electrical synapses by nature can only be produced among close neurons. The response of neuron networks has been studied for the case of an external, single spike input given by $I_i^{(e)}(t)$ with magnitude A and spike width t_w applied for $t_{in} \leqslant t < t_{in}+t_w$, $\Theta(x)$ being the Heaviside function. Added white noises $\xi_i(t)$ are given by

$$\langle \xi_i(t) \rangle = 0, \quad (7)$$

$$\langle \xi_i(t)\xi_j(t') \rangle = \beta^2 \delta_{ij}\delta(t - t'), \quad (8)$$

where the average of $\langle U(\mathbf{z},t) \rangle$ for an arbitrary function of $U(\mathbf{z},t)$ is given by

$$\langle U(\mathbf{z},t) \rangle = \int \cdots \int d\mathbf{z} U(\mathbf{z},t)\Pr(\mathbf{z}), \quad (9)$$

$\Pr(\mathbf{z})$ denoting a probability distribution function for $2N$-dimensional random variables $\mathbf{z}=(\{x_{\kappa i}\})$.

Our WS-SW network has been made after [3]. Starting from a regular network, N_{ch} couplings among $NZ/2$ couplings are randomly modified such that $c_{ij}=1$ is changed to $c_{ij}=0$ or vice versa. The coupling randomness p is given by

$$p = \frac{2N_{ch}}{NZ}, \quad (10)$$

which is 0 and 1 for completely regular and random couplings, respectively.

In the DMA [19,10], we will obtain equations of motions for means, variances, and covariances of state variables. Variables spatially averaged over the ensemble are defined by

$$X_\kappa(t) = \frac{1}{N}\sum_i x_{\kappa i}, \quad \kappa = 1,2, \quad (11)$$

and their means by

$$\mu_\kappa(t) = \langle\langle X_\kappa(t) \rangle\rangle_c, \quad (12)$$

where the brackets $\langle\cdot\rangle_c$ denote the average over the coupling configuration. As for variances and covariances of state variables, we consider three kinds of spatial correlations: (1) on-site correlation (γ), (2) the correlation for a coupled pair (ζ), and (3) that for a pair without direct couplings (η):

$$\langle\langle \delta x_{\kappa i}\delta x_{\lambda j} \rangle\rangle_c = \begin{cases} \gamma_{\kappa,\lambda}, & \text{for } i = j, \\ \zeta_{\kappa,\lambda}, & \text{for } i \neq j, \quad c_{ij} = 1, \\ \eta_{\kappa,\lambda}, & \text{for } i \neq j, \quad c_{ij} = 0, \end{cases} \quad (13)$$

where $\kappa,\lambda=1,2$ and

$$\delta x_{\kappa i}(t) = x_{\kappa i}(t) - \mu_\kappa(t). \quad (14)$$

In Eq. (13), $\gamma_{\kappa,\lambda}$, $\zeta_{\kappa,\lambda}$, and $\eta_{\kappa,\lambda}$ are defined by

$$\gamma_{\kappa,\lambda}(t) = \left\langle \frac{1}{N}\sum_i \langle \delta x_{\kappa i}(t)\delta x_{\lambda i}(t) \rangle \right\rangle_c, \quad (15)$$

$$\zeta_{\kappa,\lambda}(t) = \left\langle \frac{1}{NZ}\sum_i \sum_j c_{ij}\langle \delta x_{\kappa i}(t)\delta x_{\lambda j}(t) \rangle \right\rangle_c, \quad (16)$$

$$\eta_{\kappa,\lambda}(t) = \left\langle \frac{1}{N(N-Z-1)}\sum_i \sum_j (1 - \delta_{ij} - c_{ij}) \times \langle \delta x_{\kappa i}(t)\delta x_{\lambda j}(t) \rangle \right\rangle_c. \quad (17)$$

For a later purpose, we define also the spatially averaged correlation given by

$$\rho_{\kappa,\lambda}(t) = \left\langle \frac{1}{N^2} \sum_i \sum_j \langle \delta x_{\kappa i}(t)\, \delta x_{\lambda j}(t) \rangle \right\rangle_c \tag{18}$$

$$= \langle\langle \delta X_\kappa(t)\, \delta X_\lambda(t) \rangle\rangle_c, \tag{19}$$

where $\delta X_\kappa(t) = X_\kappa(t) - \mu_\kappa(t)$. It is noted that $\gamma_{\kappa,\lambda}$, $\zeta_{\kappa,\lambda}$ $\eta_{\kappa,\lambda}$, and $\rho_{\kappa,\lambda}$ are not independent, obeying the sum rule given by

$$N\rho_{\kappa,\lambda} = \gamma_{\kappa,\lambda} + Z\zeta_{\kappa,\lambda} + (N - Z - 1)\,\eta_{\kappa,\lambda}. \tag{20}$$

In order to derive Eqs. (15)–(20), we have employed the decomposition

$$1 = \delta_{ij} + (1 - \delta_{ij})[c_{ij} + (1 - c_{ij})] = \delta_{ij} + c_{ij} + (1 - \delta_{ij} - c_{ij}), \tag{21}$$

with $c_{ii} = 0$.

In calculating means, variances, and covariances given by Eqs. (12) and (15)–(18), we have assumed that (1) the noise intensity is weak and (2) the distribution of state variables takes the Gaussian form. By using the first assumption, we expand the DE's given by Eqs. (3)–(6) in a power series of fluctuations around means. The second assumption may be justified by some numerical calculations for stochastic FN [23,24] and HH neuron models [25,26]. It has been shown that for weak noises, the distribution of a membrane potential of a single FN or HH neuron nearly follows the Gaussian distribution, although for strong noises, the distribution deviates from the Gaussian, taking a bimodal form.

Before closing Sec. II A, we briefly summarize the introduced variables and their meanings as follows: N, the number of neurons; Z, the average coordination number; p, the coupling randomness; K, the coupling strength; c_{ij}, the adjacent matrix; X_κ, the spatially average of the fast ($\kappa = 1$) and slow ($\kappa = 2$) variables; μ_κ, a mean value of X_κ; $\gamma_{\kappa,\lambda}$, $\zeta_{\kappa,\lambda}$, and $\eta_{\kappa,\lambda}$, the correlations of on-site, a coupled pair, and an uncoupled pair, respectively.

B. Equations of motions

We will obtain equations of motions for $\mu_\kappa(t)$, $\gamma_{\kappa,\lambda}(t)$, $\zeta_{\kappa,\lambda}(t)$, $\eta_{\kappa,\lambda}(t)$, and $\rho_{\kappa,\lambda}(t)$. Readers who are not interested in mathematical details may skip to Sec. II C, where our theoretical results are summarized.

After some manipulations, we get the following DE's (the argument t being suppressed; for details; see the Appendix):

$$\frac{d\mu_1}{dt} = f_0 + f_2\gamma_{1,1} - c\mu_2 + I_{ext}, \tag{22}$$

$$\frac{d\mu_2}{dt} = b\mu_1 - d\mu_2 + e, \tag{23}$$

$$\frac{d\gamma_{1,1}}{dt} = 2(a\gamma_{1,1} - c\gamma_{1,2}) + 2KZh_1(\zeta_{1,1} - \gamma_{1,1}) + \beta^2, \tag{24}$$

$$\frac{d\gamma_{2,2}}{dt} = 2(b\gamma_{1,2} - d\gamma_{2,2}), \tag{25}$$

$$\frac{d\gamma_{1,2}}{dt} = b\gamma_{1,1} + (a - d)\gamma_{1,2} - c\gamma_{2,2} + KZh_1(\zeta_{1,2} - \gamma_{1,2}), \tag{26}$$

$$\frac{d\rho_{1,1}}{dt} = 2(a\rho_{1,1} - c\rho_{1,2}) + \frac{\beta^2}{N}, \tag{27}$$

$$\frac{d\rho_{2,2}}{dt} = 2(b\rho_{1,2} - d\rho_{2,2}), \tag{28}$$

$$\frac{d\rho_{1,2}}{dt} = b\rho_{1,1} + (a - d)\rho_{1,2} - c\rho_{2,2}, \tag{29}$$

$$\frac{d\zeta_{1,1}}{dt} = 2(a\zeta_{1,1} - c\zeta_{1,2}) + 2Kh_1[\gamma_{1,1} + (ZC - ZR)\zeta_{1,1} + (ZR - ZC - 1)\,\eta_{1,1}], \tag{30}$$

$$\frac{d\zeta_{2,2}}{dt} = 2(b\zeta_{1,2} - d\zeta_{2,2}), \tag{31}$$

$$\frac{d\zeta_{1,2}}{dt} = b\zeta_{1,1} + (a - d)\zeta_{1,2} - c\zeta_{2,2} + Kh_1[\gamma_{1,2} + (ZC - ZR)\zeta_{1,2} + (ZR - ZC - 1)\,\eta_{1,2}], \tag{32}$$

$$\frac{d\eta_{1,1}}{dt} = 2(a\eta_{1,1} - c\eta_{1,2}) + \left(\frac{2KZh_1}{N - Z - 1}\right)[(ZR - ZC - 1) \times (\zeta_{1,1} - \eta_{1,1})], \tag{33}$$

$$\frac{d\eta_{2,2}}{dt} = 2(b\eta_{1,2} - d\eta_{2,2}), \tag{34}$$

$$\frac{d\eta_{1,2}}{dt} = b\eta_{1,1} + (a - d)\eta_{1,2} - c\eta_{2,2} + \left(\frac{KZh_1}{N - Z - 1}\right) \times [(ZR - ZC - 1)(\zeta_{1,2} - \eta_{1,2})], \tag{35}$$

with

$$C = \left\langle \frac{1}{NZ^2} \sum_i \sum_j \sum_k c_{ij}c_{jk}c_{ik} \right\rangle_c, \tag{36}$$

$$R = \left\langle \frac{1}{NZ^2} \sum_i \sum_j \sum_k c_{ij}c_{jk} \right\rangle_c, \tag{37}$$

where $a = f_1 + 3f_3\gamma_{1,1}$, $f_\ell = (1//\ell!)F^{(\ell)}$ and $h_1 = H^{(1)}(0)$ with $H(0) = H^{(2)}(0) = 0$.

C. Summary of our method

The clustering coefficient C and the coupling connectivity R, which are given by Eqs. (36) and (37), respectively, play important roles in our DMA theory for SW networks. The clustering coefficient C introduced in SW networks [3,4] expresses a factor forming a cluster where the three sites i, j,

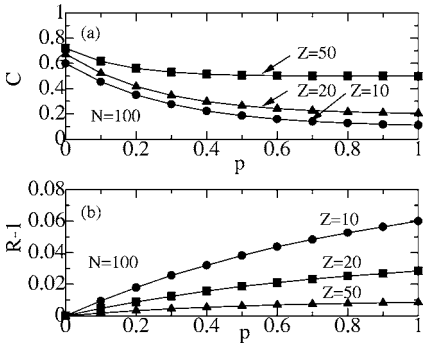

FIG. 1. The coupling randomness (p) dependence of (a) the clustering coefficient C and (b) the coupling connectivity R of SW networks for $Z=10$, 20, and 50 with $N=100$.

and k are mutually coupled. In contrast, the coupling connectivity R expresses a factor for a cluster where the two sites j and k are coupled to the third site i, but the sites j and k are not necessarily coupled.[1] It is noted in Eqs. (22)–(35) that there is no explicit dependence on the coupling randomness p and it is only through parameters C and R in the mean-field equations.

Figures 1(a) and 1(b) show the p dependences of C and R, respectively, for various Z values with $N=100$. With increasing p from zero, C is decreased and approaches $C=Z/N$ at $p=1$. In contrast, R is monotonically increased with increasing p.

Among the 12 correlations such as $\gamma_{\kappa,\lambda}$, etc., given by Eqs. (15)–(18), nine correlations are independent because of the sum rule given by Eq. (20). In this study, we have chosen nine correlations of $\gamma_{\kappa,\lambda}$, $\zeta_{\kappa,\lambda}$, and $\rho_{\kappa,\lambda}$ as independent variables. Then the original $2N$-dimensional *stochastic* DE's given by Eqs. (3) and (4) have been transformed to 11-dimensional *deterministic* DE's. Equations of motions for diffusive couplings given by Eqs. (22)–(35) are rather different from those for sigmoid couplings given by Eqs. (21)–(34) in [10], a related discussion being given in Sec. IV.

From a comparison of Eq. (24) with Eq. (27), we note that

$$\rho_{1,1} = \frac{\gamma_{1,1}}{N} \quad (\text{for } K/\beta \to 0) \tag{38}$$

$$= \gamma_{1,1} \quad (\text{for } \beta/K \to 0), \tag{39}$$

where Eq. (38) is nothing but the central-limit theorem describing the relation between fluctuations of local and average variables [Eqs. (15) and (19)]. In order to quantitatively discuss the synchronization, we first consider the quantity given by

$$P(t) = \frac{1}{N^2}\sum_{ij} \langle [x_{1i}(t) - x_{1j}(t)]^2 \rangle = 2[\gamma_{1,1}(t) - \rho_{1,1}(t)]. \tag{40}$$

When all neurons are in the completely synchronous state, we get $x_{1i}(t)=X_1(t)$ for all i and then $P(t)=0$ in Eq. (40). On the contrary, in the asynchronous state, we get $P(t)=2(1-1/N)\gamma_{1,1} \equiv P_0(t)$ from Eq. (38). We have defined the synchronization ratio given by [10]

$$S(t) = 1 - \frac{P(t)}{P_0(t)} = \left(\frac{N\rho_{1,1}(t)/\gamma_{1,1}(t) - 1}{N-1} \right), \tag{41}$$

which is 0 and 1 for completely asynchronous ($P=P_0$) and synchronous states ($P=0$), respectively.

We define the time t_{max} when $S(t)$ takes its maximum value as

$$t_{max} = \{t | dS(t)/dt = 0, t_{in} \leqslant t \leqslant t_{in} + t_w\}. \tag{42}$$

The maximum value of $S_{max}[=S(t_{max})]$ depends on model parameters such as the coupling strength (K), the noise intensity (β), the size of cluster (N), the coordination number (Z), and the coupling randomness (p), as will be discussed in the following section.

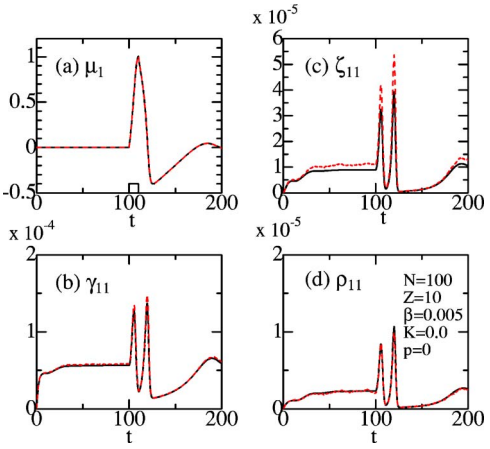

FIG. 2. (Color online) Time courses of (a) μ_1, (b) $\gamma_{1,1}$, (c) $\zeta_{1,1}$, and (d) $\rho_{1,1}$ for $\beta=0.005$, $K=0.02$, $N=100$, $Z=10$, and $p=0.0$, solid and dashed curves denoting results of DMA and direct simulations, respectively. At the bottom of (a), an input signal is plotted. Vertical scales of (b), (c), and (d) are multiplied by factors of 10^{-4}, 10^{-5}, and 10^{-5}, respectively.

III. CALCULATED RESULTS

A. Regular couplings

We have adopted same parameters of $\theta=0.5$, $\alpha=0.5$, $\tau_s=10$, $A=0.10$, $t_{in}=100$, and $T_w=10$ as in [19] and the H function given by

$$H(x_{1j} - x_{1j}) = x_{1j} - x_{1j}. \tag{43}$$

DMA calculations have been made by solving Eqs. (22)–(35) with the use of the fourth-order Runge-Kutta method with a time step of 0.01. We have performed also direct simulations by using the fourth-order Runge-Kutta method with a time step of 0.01. The results of direct simulations are averages of 1000 trials for $Z \leqslant 20$ and those of 100 trials otherwise noticed. All quantities are dimensionless.

First we discuss the case of regular couplings ($p=0.0$). Figures 2(a)–2(d) show time courses of μ_1, $\gamma_{1,1}$, $\zeta_{1,1}$, and

[1]What is customarily called the clustering coefficient corresponds to C/R where C and R are defined by Eqs. (36) and (37), respectively, in the present paper [1].

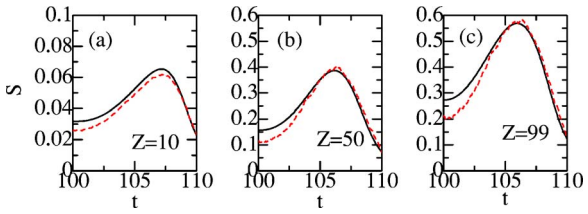

FIG. 3. (Color online) Time courses of $S(t)$ for (a) $Z=10$, (b) $Z=50$, and (c) $Z=99$ calculated by DMA (solid curves) and direct simulations (dashed curves) ($\beta=0.005$, $K=0.02$, $N=100$, and $p=0.0$).

$\rho_{1,1}$, respectively, with $\beta=0.005$, $K=0.02$, $p=0.0$, $N=100$, and $Z=10$. Results of the DMA expressed by solid curves are in good agreement with those of direct simulations depicted by dashed curves. The time courses of μ_1, $\gamma_{1,1}$ $\zeta_{1,1}$, and $\rho_{1,1}$ shown in Figs. 2(a)–2(d) are not so different from those for sigmoid couplings reported in Figs. 3(a)–3(d) of [10].

Figures 3(a)–3(c) show time courses of $S(t)$ calculated by DMA (solid curves) and direct simulations (dashed curves) for $Z=10$, 50, and 99, whose magnitudes are increased with increasing Z. The maximum values of the synchronization ratio in the DMA are 0.0654, 0.386, and 0.569 for $Z=10$, 50, and 99, respectively, which shows a larger synchrony for larger Z. This is more clearly seen in Fig. 4(a) showing S_{max} as a function of Z. Figure 4(b) shows the Z dependences of $\gamma_{1,1}$, $\zeta_{1,1}$, and $\rho_{1,1}$ at $t=t_{max}$ with $K=0.02$, $\beta=0.005$, and $N=100$: solid and open marks express results of DMA and direct simulations, respectively. With increasing Z, $\gamma_{1,1}$ is significantly decreased while $\rho_{1,1}$ and $\zeta_{1,1}$ are almost constant. This explains the larger synchrony S_f for larger Z, shown in Fig. 4(a). The difference between the Z dependences of $\gamma_{1,1}$ and $\rho_{1,1}$ is due to the fact that $d\gamma_{1,1}/dt$ has a contribution from the second term of $2KZh_1(\zeta_{1,1}-\gamma_{1,1})$ in Eq. (24) while $d\rho_{1,1}/dt$ has no such contributions in Eq. (27). Figure 4(b) shows that $\zeta_{1,1}$ also depends on Z because of the second term in Eq. (30). It is noted that because t_{max}

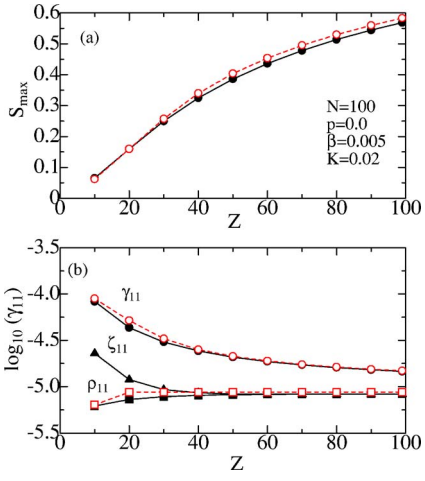

FIG. 4. (Color online) The average coordination-number (Z) dependence of (a) S_{max} and (b) $\gamma_{1,1}$ (circles), $\zeta_{1,1}$ (triangles), and $\rho_{1,1}$ (squares) at $t=t_{max}$ for $\beta=0.005$, $K=0.02$, $N=100$, and $p=0.0$: solid and open marks denote results of DMA and direct simulations, respectively.

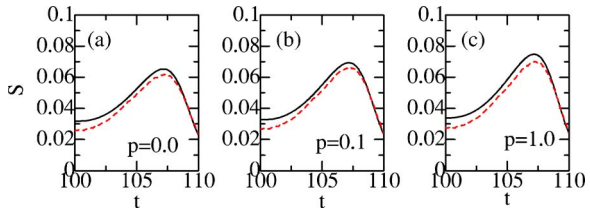

FIG. 5. (Color online) Time courses of $S(t)$ for (a) $p=0.0$, (b) 0.1, and (c) 1.0 calculated by DMA (solid curves) and direct simulations (dashed curves) ($\beta=0.005$, $K=0.02$, and $N=100$).

defined by Eq. (42) depends on Z in general, $\gamma_{1,1}$ at $t=t_{max}$ may show a weak Z dependence, as shown in Fig. 4(b) where $t_{max}=107.16$, 106.72, 106.46, and 105.96 for $Z=10$, 20, 50, and 99, respectively.

B. SW couplings

Next we discuss the case of SW couplings by changing the coupling randomness p. Figures 5(a)–5(c) show time courses of $S(t)$ for $p=0.0$, 0.1, and 1.0, respectively, calculated by DMA (solid curves) and direct simulations (dashed curves). The maximum values of the synchronization ratio S_{max} in the DMA are 0.0654, 0.0694, and 0.0749, for $p=0.0$, 0.1, and 1.0, respectively: S_{max} is slightly increased with increasing p. This p dependence of S_{max} is more clearly seen in Fig. 6(a) where S_{max} is plotted against p for $Z=10$. Figure 6(b) shows the p dependences of $\gamma_{1,1}$, $\zeta_{1,1}$, and $\rho_{1,1}$ at $t=t_{max}$ with $K=0.02$, $\beta=0.005$, $N=100$, and $Z=10$: solid and open marks express results of DMA and direct simulations, respectively. With increasing p, $\gamma_{1,1}$ is slightly decreased while $\rho_{1,1}$ is not changed. The origin of the difference between the p dependences of $\gamma_{1,1}$ and $\rho_{1,1}$ is again due to the fact that $d\gamma_{1,1}/dt$ has a contribution from the second term of $2KZh_1(\zeta_{1,1}-\gamma_{1,1})$ in Eq. (24) while $d\rho_{1,1}/dt$ has no such contributions in Eq. (27): the p dependence of $\gamma_{1,1}$ arises from $\zeta_{1,1}$ which depends on p through network parameters of C and R in Eq. (30), as shown in Fig. 6(b).

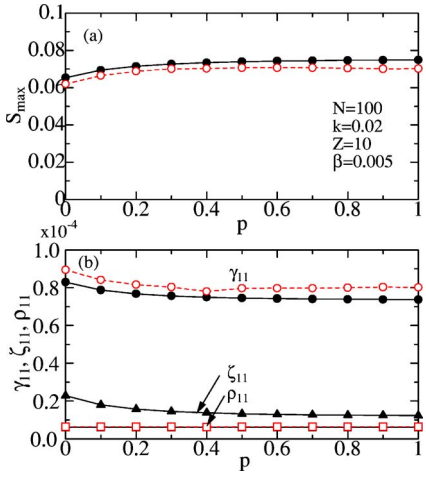

FIG. 6. (Color online) The coupling randomness (p) dependence of (a) S_{max} and (b) $\gamma_{1,1}$ (circles), $\zeta_{1,1}$ (triangles), and $\rho_{1,1}$ (squares) at $t=t_{max}$ for $\beta=0.005$, $K=0.02$, $N=100$, and $Z=10$: solid and open marks denote results of DMA and direct simulations, respectively.

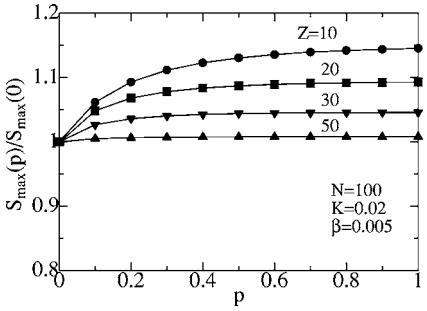

FIG. 7. The coupling randomness (p) dependence of $S_{max}(p)/S_{max}(0)$ for $Z=10$, 20, and 50 and with $\beta=0.005$, $K=0.02$, and $N=100$.

In Fig. 7, $S_{max}(p)$ normalized by its $p=0.0$ value is plotted for various Z with $N=100$, $K=0.02$, and $\beta=0.005$. Values of $S_{max}(p=0.1)/S_{max}(p=0.0)$ in the DMA are 1.061, 1.048, 1.0268, and 1.000 for $Z=10$, 20, 30, and 50, respectively: an increase in S_{max} is larger for smaller Z.

IV. CONCLUSION AND DISCUSSION

Calculations in the preceding subsection show that when the coupling randomness p is introduced to regular networks, the synchronization may be slightly increased for diffusive couplings. This is in strong contrast with the result for sigmoid couplings in [10], which shows a decreased synchronization with increasing the coupling randomness. The main origin of an increased synchronization for diffusive couplings may be their local negative feedback, as will be discussed in the followings. The diffusive coupling given by Eqs. (5) and (43) may be rewritten as

$$I_i^{(c)}(t) = K\sum_j c_{ij}(x_{1j} - x_{1i}) = K\left(\sum_j c_{ij}x_{1j} - k_i x_{1i}\right), \quad (44)$$

where $k_i(=\Sigma_j c_{ij})$ is heterogeneous. We may show that the heterogeneity in the coordination number k_i of Eq. (44) plays an important role in an increase of S_{max} of SW networks. If we replace k_i by its average of $Z(=\langle k_i\rangle)$ in the feedback term of Eq. (44), it becomes

$$I_i^{(c)}(t) \sim K\left(\sum_j c_{ij}x_{1j} - Zx_{1i}\right). \quad (45)$$

The solid and open circles in Fig. 8 denote S_{max} calculated by using Eq. (44) with DMA and simulations, respectively, for $N=100$, $Z=10$, $\beta=0.005$, and $K=0.02$. The solid and open squares in Fig. 8 express S_{max} calculated by using Eq. (45) with DMA and direct simulations, respectively, for the same parameters as mentioned above. Figure 8 clearly shows that heterogeneous negative-feedback term $(-Kk_i x_{1i})$ in Eq. (44) leads to a slightly increased synchronization whereas the homogeneous one $(-KZx_{1i})$ in Eq. (45) yields a decreased synchronization.

Equation (44) may be alternatively rewritten as

$$I_i^{(c)}(t) = K\sum_j d_{ij}x_{1j}, \quad (46)$$

with

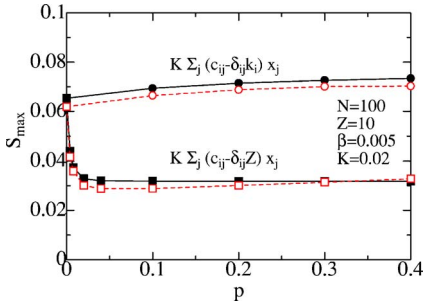

FIG. 8. (Color online) The coupling randomness (p) dependence of S_{max} for the couplings $K\Sigma_j(c_{ij}-\delta_{ij}k_i)x_{1j}$ (circles) and $K\Sigma_j(c_{ij}-\delta_{ij}Z)x_{1j}$ (squares) with $N=100$, $Z=10$, $\beta=0.005$, and $K=0.02$, solid and open marks denoting the results of DMA and direct simulations, respectively (see text).

$$d_{ij} = c_{ij} - \delta_{ij}k_i. \quad (47)$$

It is noted that the new adjacent matrix d_{ij} given by Eq. (47) satisfies the relation given by

$$\sum_j d_{ij} = 0. \quad (48)$$

Nishikawa *et al.* [17] have studied the stability of synchronous states of coupled networks in which the adjacent (Laplacian) matrix is assumed to satisfy the relation as given by Eq. (48). This implies that the coupling adopted in [17] is related to a diffusive process. From an analysis of the stability of the synchronous state by the Lyapunov index, they have shown that the synchronization becomes more difficult in SW and SF networks with more heterogeneity. Our calculation is expected not to be in contradiction with theirs because they examine the criteria for the stability of synchronous oscillations while we have discussed the degree of synchronization for an applied signal. It has been conventionally claimed that an increase in the synchronization arises from the short average distance L in SW networks [7,11,13–15]. However, the equations of motions presented in Eqs. (22)–(35) (and those in [10]) do not include the term relevant to L of SW networks.

There is also the difference between effects of heterogeneity for sigmoid and diffusive couplings. For sigmoid couplings [10], the effect of the heterogeneity of SW networks is included by a perturbation method with the term of $\delta c_{ij}[=c_{ij}(p)-c_{ij}(p=0)]$ through new correlations functions of ϕ_1 and ϕ_2 [see Eq. (37) in [10]]. This has been made because the term $\langle \delta x_{1i}\delta c_{ij}\rangle$ appears in the process of calculating equations of motion, for example, of $d\gamma_{1,1}/dt$. In contrast, for the diffusive couplings, the counterpart term becomes $\langle \delta x_{1i}\delta x_{1j}\delta c_{ij}\rangle$, which is in a higher order than $\langle \delta x_{1i}\delta c_{ij}\rangle$. This shows that the effect of heterogeneity for diffusive couplings is weaker than that for sigmoid couplings: for the diffusive couplings its effect may be included by the p-dependent C and R in the mean-field approximation, while for sigmoid couplings it has to be taken into account by the perturbation method. The stronger heterogeneity for the sigmoid couplings yields a decrease in the synchronization when the heterogeneity is introduced.

To summarize, we have discussed the synchronization in SW networks of spiking FN neurons with diffusive couplings, employing the semianalytical DMA theory previously developed in [10]. A comparison of the results in this calculation with those for sigmoid couplings in [10] leads to the following results.

(1) When the average coordination number Z is increased, the synchronization S is increased both for sigmoid and diffusive couplings. We should note, however, that an increase in S is mainly made by an increase in $\rho_{1,1}$ for sigmoid couplings [Fig. 4(a) in [10]] while it is accomplished by a decrease in $\gamma_{1,1}$ for diffusive couplings [Fig. 4(b) in this paper].

(2) When the coupling randomness p is increased, the synchronization S is decreased by an introduced heterogeneity for sigmoid couplings, whereas for diffusive couplings, S may be slightly increased by their negative local feedback contribution which compensates its decrease caused by their heterogeneity.

It is noted that an increase in the synchronization of item (2) is due to local negative feedback in diffusive couplings, but not due to the short average distance in SW networks, against the conventional wisdom. Item (2) is consistent with the results in SW networks of the phase model with the coupling term of $H(x-y)=\sin(x-y)$, for which an increase in the synchronization with increasing p has been reported [13,14]. Items (1) and (2) imply that the synchronization of SW networks depends not only on the geometry of SW networks but also on details of couplings. In the present paper, we have neglected the transmission time delay. Because the average path length becomes shorter by added shortcuts [3,4], the response speed is expected to be improved in SW networks with time delays. This is a great advantage of SW networks though the synchronization may be not necessarily improved. The discussions in this paper and [10] have been confined to SW neural networks with symmetric (undirected) and unweighted couplings. Recently it has been shown that the synchronization in complex networks may be enhanced if their couplings are undirected and weighted [18]. It is interesting to apply our semianalytical approach to networks with directed and weighted couplings, which are realized in real complex networks. This subject is left as our future study.

ACKNOWLEDGMENTS

This work is partly supported by a Grant-in-Aid for Scientific Research from the Japanese Ministry of Education, Culture, Sports, Science and Technology.

APPENDIX: DERIVATION OF EQS. (22)–(35)

Substituting Eq. (14) into Eqs. (3)–(6), we get DE's for δx_{1i} and δx_{2i} of a neuron i, given by (argument t is suppressed)

$$\frac{d\delta x_{1i}}{dt} = f_1 \delta x_{1i} + f_2(\delta x_{1i}^2 - \gamma_{1,1}) + f_3 \delta x_{1i}^3 - c\,\delta x_{2i} + \delta I_i^{(c)} + \xi_j, \tag{A1}$$

$$\frac{d\delta x_{2j}}{dt} = b\,\delta x_{1j} - d\,\delta x_{2j}, \tag{A2}$$

with

$$\delta I_i^{(c)}(t) = K\sum_j c_{ij}\{h_1[\delta x_{1j}(t) - \delta x_{1j}(t)] + h_3[\delta x_{1j}(t) - \delta x_{1j}(t)]^3\}, \tag{A3}$$

where $f_\ell = (1/\ell!)F^{(\ell)}$ and $h_\ell = (1/\ell!)H^{(\ell)}$. DE's for the correlations are given by

$$\frac{d\gamma_{\kappa,\lambda}}{dt} = \left\langle \frac{1}{N}\sum_i \left\langle \left[\delta x_{\kappa i}\left(\frac{d\delta x_{\lambda i}}{dt}\right) + \left(\frac{d\delta x_{\kappa i}}{dt}\right)\delta x_{\lambda i}\right]\right\rangle\right\rangle_c, \tag{A4}$$

$$\frac{d\zeta_{\kappa,\lambda}}{dt} = \left\langle \frac{1}{NZ}\sum_i \sum_j c_{ij}\left\langle \left[\delta x_{\kappa i}\left(\frac{d\delta x_{\lambda j}}{dt}\right) + \left(\frac{d\delta x_{\kappa j}}{dt}\right)\delta x_{\lambda i}\right]\right\rangle\right\rangle_c, \tag{A5}$$

$$\frac{d\rho_{\kappa,\lambda}}{dt} = \left\langle \frac{1}{N^2}\sum_i \sum_j \left\langle \left[\delta x_{\kappa i}\left(\frac{d\delta x_{\lambda j}}{dt}\right) + \left(\frac{d\delta x_{\kappa j}}{dt}\right)\delta x_{\lambda i}\right]\right\rangle\right\rangle_c. \tag{A6}$$

With the use of Eqs. (A4)–(A6), we may calculate DE's given by Eqs. (22)–(35). For example, terms including $\delta I_i^{(e)}$ in $d\gamma_{1,1}/dt$, $d\zeta_{1,1}/dt$, and $d\rho_{1,1}/dt$ become

$$\left\langle \frac{2}{N}\sum_i \langle \delta x_{1i}\delta I_i^{(c)}\rangle \right\rangle_c = \frac{2Kh_1}{N}\sum_i \sum_j \langle\langle c_{ij}\delta x_{1i}[\delta x_{1j} - \delta x_{1i}]\rangle\rangle_c \tag{A7}$$

$$= 2KZh_1(\zeta_{1,1} - \gamma_{1,1}), \tag{A8}$$

$$\left\langle \frac{2}{NZ}\sum_i \sum_j c_{ij}\langle \delta x_{1i}\delta I_j^{(c)}\rangle \right\rangle_c = \frac{2Kh_1}{NZ}\sum_i \sum_j \sum_k \langle\langle c_{ij}c_{jk}\delta x_{1i}[\delta x_{1k} - \delta x_{1j}]\rangle\rangle_c \tag{A9}$$

$$= \frac{2KZh_1}{N}[\gamma_{1,1} + Z(C-R)\zeta_{1,1} + (ZR - ZC - 1)\eta_{1,1}], \tag{A10}$$

$$\left\langle \frac{2}{N^2}\sum_i \sum_j \langle \delta x_{1i}\delta I_j^{(c)}\rangle \right\rangle_c = \frac{2Kh_1}{N^2}\sum_i \sum_j \sum_k \langle\langle c_{jk}\delta x_{1i}[\delta x_{1k} - \delta x_{1j}]\rangle\rangle_c \tag{A11}$$

$$= 0. \tag{A12}$$

In evaluating Eqs. (A7)–(A12), we have employed the relation given by Eq. (13):

$$\langle\langle \delta x_{\kappa i}\delta x_{\lambda j}\rangle\rangle_c = \gamma_{\kappa,\lambda}\delta_{ij} + \zeta_{\kappa,\lambda}c_{ij} + \eta_{\kappa,\lambda}(1 - \delta_{ij} - c_{ij}). \tag{A13}$$

[1] R. Albert and A. Barabási, Rev. Mod. Phys. **74**, 47 (2002).
[2] S. N. Dorogovtsev and J. F. F. Mendes, Adv. Phys. **51**, 1079 (2002).
[3] D. J. Watts and S. H. Strogatz, Nature (London) **393**, 440 (1998).
[4] S. H. Strogatz, Nature (London) **410**, 268 (2001).
[5] M. E. J. Newman and D. J. Watts, Phys. Lett. A **263**, 341 (1999).
[6] A. Barabási and R. Albert, Nature (London) **286**, 509 (1999).
[7] L. F. Lago-Fernández, R. Huerta, F. Corbacho, and J. A. Sigüenza, Phys. Rev. Lett. **84**, 2758 (2000).
[8] T. I. Netoff, R. Clewley, S. Arno, T. Keck, and J. A. White, J. Neurosci. **24**, 8075 (2004).
[9] L. F. Lago-Fernández, F. J. Corbacho, and R. Huerta, Neural Networks **14**, 687 (2001).
[10] H. Hasegawa, Phys. Rev. E **70**, 066107 (2004).
[11] M. Bucolo, L. Fortuna, and M. La Rosa, Chaos, Solitons Fractals **14**, 1059 (2002).
[12] N. Masuda and K. Aihara, Biol. Cybern. **90**, 302 (2004).
[13] H. Hong, M. Y. Choi, and B. J. Kim, Phys. Rev. E **65**, 026139 (2002).
[14] H. Hong, M. Y. Choi, and B. J. Kim, Phys. Rev. E **65**, 047104 (2002).
[15] G. Buzsáki, C. Geisler, D. A. Henze, and X.-J. Wang, Trends Neurosci. **27**, 186 (2004).
[16] M. Barahona and L. M. Pecora, Phys. Rev. Lett. **89**, 054101 (2002).
[17] T. Nishikawa, A. E. Motter, Y. C. Lai, and F. C. Hoppensteadt, Phys. Rev. Lett. **91**, 014101 (2003).
[18] A. E. Motter, C. Zhou, and J. Kurths, Europhys. Lett. **69**, 334 (2005); Phys. Rev. E **71**, 016116 (2005).
[19] H. Hasegawa, Phys. Rev. E **67**, 041903 (2003).
[20] H. Hasegawa, Phys. Rev. E **68**, 041909 (2003).
[21] J. R. Gibson and B. W. Connors, in *The Handbook of Brain Theory and Neural Networks*, edited by M. A. Arbib (MIT Press, Cambridge, MA, 2003), pp. 725–729.
[22] R. Rodriguez and H. C. Tuckwell, Phys. Rev. E **54**, 5585 (1996).
[23] H. C. Tuckwell and R. Rodriguez, J. Comput. Neurosci. **5**, 91 (1998).
[24] S. Tanabe and K. Pakdaman, Phys. Rev. E **63**, 031911 (2001).
[25] S. Tanabe, S. Sato, and K. Pakdaman, Phys. Rev. E **60**, 7235 (1999).
[26] S. Tanabe and K. Pakdaman, Biol. Cybern. **85**, 269 (2001).